In vitro Apatite mineralization and heat generation of magnetite-reduced graphene oxide nanocomposites for hyperthermia treatment

Toshiki Miyazaki[a], Jun Akaike[a], Masakazu Kawashita[b] and Hong Ngee Lim[c]

[a]Graduate School of Life Science and System Engineering, Kyushu Institute of Technology, 2-4, Hibikino, Wakamatsu-ku, Kitakyushu 808-0196

[b]Graduate School of Biomedical Engineering, Tohoku University, 6-6-12-209, Aramaki, Aoba, Aoba-ku, Sendai 980-8579, Japan

[c]Department of Chemistry, Faculty of Science, Universiti Putra Malaysia, 43400 UPM Serdang, Selangor, Malaysia

Corresponding author:
Toshiki Miyazaki
Graduate School of Life Science and Systems Engineering, Kyushu Institute of Technology, 2-4, Hibikino, Wakamatsu-ku, Kitakyushu 808-0196, Japan
Tel/Fax: +81-93-695-6025
E-mail: tmiya@life.kyutech.ac.jp

Abstract

Nanocomposites of magnetite (Fe_3O_4) and reduced graphene oxide (rGO) generate heat under an alternating magnetic field and therefore have potential applications as thermoseeds for cancer hyperthermia treatment. However, the properties of such nanocomposites as biomaterials have not been sufficiently well characterized. In this study, the osteoconductivity of Fe_3O_4-rGO nanocomposites of various compositions was evaluated *in vitro* in terms of their apatite-forming ability in simulated body fluid (SBF). Furthermore, the heat generation of the nanocomposites was measured under an alternating magnetic field. The apatite-forming ability in SBF improved as the Fe_3O_4 content in the nanocomposite was increased. As the Fe_3O_4 content was increased, the nanocomposite not only rapidly raised the surrounding temperature to approximately 100°C, but the specific absorption rate also increased. We assumed that the ionic interaction between the Fe_3O_4 and rGO was enhanced and that Brown relaxation was suppressed as the proportion of rGO in the nanocomposite was increased. Consequently, a high content of Fe_3O_4 in the nanocomposite was effective for improving both the osteoconductivity and heat generation characteristics for hyperthermia applications.

Keywords

Magnetite, Graphene oxide, Simulated body fluid, Apatite, Heat generation, Hyperthermia treatment

1. Introduction

Magnetic nanoparticles, such as magnetite (Fe_3O_4), generate heat under an alternating magnetic field. This effect has drawn attention for potential applications to thermoseeds for hyperthermia treatment of deep-seated tumors [1]. This treatment is based on the fact that cancer cells are more vulnerable to heat than normal cells. The nanoparticles can be injected directly into the tumor in a clinical treatment. Microspheres, agglutinated to approximately 20–30 μm in size, also show an embolotherapeutic effect, which blocks the blood flow around the cancer and weakens the tumor [2,3]. Furthermore, if the magnetic nanoparticles have bone-bonding properties (osteoconductivity), they can be stably fixed in bone defects and are useful for treatment of bone tumors. For this purpose, research has been conducted on FeO-Fe_2O_3-CaO-SiO_2 osteoconductive glass ceramics [4], apatite-Fe_3O_4 composites [5], and calcium phosphate cements with added Fe_3O_4 [6].

Graphene has also attracted considerable attention as a biomaterial because of its excellent cell adhesion [7]. The application of graphene to photodynamic therapy has been studied owing to its excellent light absorption properties in near infrared region [8].

Composites of Fe_3O_4 and graphene are expected to behave as thermoseeds with excellent biocompatibility and heat transfer characteristics [9]. It has been reported that materials with carboxyl groups induce bone-like apatite formation in the body and exhibit osteoconductivity [10,11,12]. Graphene oxide (GO) and reduced graphene oxide (rGO), which feature hydrophilic carboxyl groups on their surfaces, are also expected to have excellent compatibility with bone tissue.

Lim *et al.* synthesized Fe_3O_4-rGO nanocomposites by an aqueous process and investigated the decomposition behavior of adsorbed dye under the photocatalytic effect of sunlight [13,14]. Ye *et al.* investigated protein adsorption and magnetization behavior of a GO-Fe_3O_4-chitosan composite [15]. However, the effects of the composition of this material on heat generation properties and osteoconductivity were not investigated in detail.

In this study, the osteoconductivity of a Fe_3O_4-rGO nanocomposite with different Fe_3O_4/rGO ratios was evaluated by *in vitro* testing in simulated body fluid (SBF). Additionally, the change in temperature was measured under irradiation by an

alternating magnetic field, and the heat generation ability is discussed in terms of the specific absorption rate (SAR) and the chemical structure of the nanocomposites.

2. Materials and methods

2.1 Preparation of Fe_3O_4-rGO nanocomposites

Fe_3O_4-rGO nanocomposites were prepared according to previous reports [13,16]. Briefly, graphite was oxidized with sulfuric acid and potassium permanganate. The obtained GO was dispersed in an aqueous solution of ammonia and iron (II) sulfate, and stirred for 1 day to obtain the nanocomposite. GO is thought to be partially reduced by Fe^{2+} in this process. We produced samples with rGO : iron sulfate mass ratios of 1 : *x*, hereafter denoted as GF*x*. A sample without rGO was also prepared (denoted as F). Graphite flakes were purchased from Ashbury Carbons Inc. (NJ, USA) Sulfuric acid, potassium permanganate, iron (II) sulfate heptahydrate, and ammonia solution were purchased from Systerm (Selangor Darul Ehsan, Malaysia). The zeta potential of the samples in 10-mM NaCl solution was measured with a zeta-potential analyzer (ELSZ-2, Otsuka Electronics Co., Osaka, Japan) connected to a box-like quartz cell.

2.2 Soaking in SBF

The nanocomposite powder was fixed to carbon tape and stuck on a glass slide 10 × 10 × 1 mm^3 in size. The glass slides with the immobilized nanocomposite were soaked in 30 mL of SBF containing the following inorganic ion concentrations: 142.0 mM Na^+, 5.0 mM K^+, 1.5 mM Mg^{2+}, 2.5 mM Ca^{2+}, 147.8 mM Cl^-, 4.2 mM HCO_3^-, 1.0 mM HPO_4^{2-}, and 0.5 mM SO_4^{2-} [17]. The solutions were maintained at 36.5 °C for various periods and the pH of the solutions was buffered at 7.40 by 50 mM tris(hydroxymethyl)aminomethane and an appropriate amount of HCl. All reagents used for preparing SBF were purchased from Nacalai Tesque Inc. (Kyoto, Japan). After soaking, the samples were removed from the SBF, and then immersed in ultrapure water to remove excess water-soluble salts on their surface.

The surface morphology and elemental composition were characterized by energy dispersive X-ray spectroscopy (EDX; EMAX Energy system, Horiba Ltd., Kyoto, Japan) equipped to a scanning electron microscope (SEM; S-3500N, Hitachi Co., Tokyo, Japan). The Ca/P molar ratio was measured by EDX and corrected against a sintered

hydroxyapatite standard. Crystalline structures of the samples were characterized by thin-film X-ray diffraction (TF-XRD; MXP3V, Mac Science, Co., Yokohama, Japan). Monochromated Cu-Kα radiation was used for the TF-XRD analysis, which was fixed at 1° against the surface of each specimen with a scan rate of $0.02°\cdot s^{-1}$.

2.3 *In vitro* heat generation

In vitro heat generated was measured from the obtained samples subjected to a magnetic core-type alternating magnetic field generator. Full details of the construction of the apparatus have been previously reported [18]. The frequency and strength of the alternating magnetic field were fixed at 100 kHz and 23.9 $kA\cdot m^{-1}$ (300 Oe), respectively. A glass bottle containing agar phantoms and samples of the composite was placed between the coils. The agar phantom was prepared by solidification of 3 cm^3 of an aqueous solution of 1-mass% agar ultrasonically dispersed with the sample of 200 mg. Changes in the temperature of the agar phantom near the microcapsules was quantitatively measured by a fiber optic temperature sensor (OTG-MPK5, Opsens Inc.,

Quebec, Canada) attached to a signal conditioner (TempSens, Opsens Inc., Quebec, Canada). The SAR was calculated by the following equation:

$$SAR = \frac{\sum_i c_i m_i}{m_{Fe}} \frac{\Delta T}{\Delta t} \quad (1)$$

where c_i and m_i are heat capacity (C_{agar} = 4.2 J/g·K, C_{Fe3O4} = 0.937 J/g·K, C_{GO} = 0.710 J/g·K) and the mass of each component, respectively, and ΔT/Δt is initial gradient of the time-dependent temperature curve (Δt = 60 s) [19,20] Concentration of the sample used for SAR calculation was the same as *in vitro* heat generation (66.7 mg/mL).

3. Results and Discussion

3.1 *In vitro* apatite formation in SBF

Figure 1 shows SEM photographs of the sample surfaces immersed in SBF for 7 days. Spherical precipitates were observed for all the samples. Coverage ratio of the precipitates on the samples tended to increase as the Fe_3O_4 content was increased.

Figure 2 shows TF-XRD patterns of the sample surfaces immersed in SBF for 7 days. Diffraction peaks of Fe_3O_4 was observed at 30, 35 and 43° for all the samples, and broad peaks assigned to apatite of low-crystallinity were observed at 32° for GF15 and

F. This result indicates that the spherical particles observed in Fig. 1 were composed of apatite of low-crystallinity.

Table 1 shows zeta potentials of the samples. The zeta potentials were negative except for that of sample F and tended to increase as the Fe_3O_4 content was increased.

The Ca/P ratio on the samples after 2-h immersion in SBF was also shown in Table 1. It tended to decrease as the Fe_3O_4 content in the sample increased. This means that Ca and P were adsorbed to all the nanocomposite surfaces in SBF within 2 h, and that the relative amount of adsorbed P increased with increasing Fe_3O_4 content.

It was found that the Fe_3O_4-rGO nanocomposite formed apatite in SBF (See Figs. 1 and 2). rGO contains carboxyl group although its amount is lower than that of GO [16]. The carboxyl group would induce the heterogeneous apatite nucleation. In addition, Kato *et al.* reported that specific kinds of iron oxide particle have the ability to induce calcium phosphate mineralization in SBF [21]. Therefore, it is assumed that not only the carboxyl group but also Fe-OH group contribute to the apatite formation on the present nanocomposites.

The apatite formation tended to be enhanced as the Fe_3O_4 content increased (See Figs. 1 and 2). After a 2-h immersion in SBF, the samples with higher Fe_3O_4 content adsorbed a larger amount of P (See Table 1). Therefore, we assume that P adsorption at the early stage of immersion is a key factor, which triggers apatite formation. According to the zeta potential measurements, samples with lower Fe_3O_4 content were more negatively charged (See Table 1). This is attributed to the presence of carboxyl group derived from rGO. It is thought that Ca is tightly adsorbed on the highly negatively charged surfaces in SBF and that P adsorption and subsequent apatite nucleation are suppressed.

Similar phenomena have been reported by several researchers. Tavafoghi *et al* [22]. immobilized glutamic acid and arginine on GO and investigated the behavior of these composites in SBF. The sample immobilized with arginine formed a larger amount of apatite over a shorter period than that immobilized with glutamic acid. When the glutamic acid was immobilized, formation of a complex with phosphate was presumed to be suppressed by tight interactions between the carboxyl groups and Ca^{2+}. Rhee *et al*. soaked collagen films in 1.5SBF, solution with ion concentration 1.5 times of SBF,

added with citric acid [23]. Apatite formation on the collagen was suppressed when concentration of the citric acid exceeds 4.0 M. This is because Ca^{2+} and the carboxyl groups in two citric acid molecules construct stable complex. We have also investigated apatite formation on pectin, a polysaccharide containing carboxyl groups, in SBF [24]. Normal pectin formed apatite; however, pectic acid, in which all the methyl esters of pectin were converted to carboxyl groups, did not form any apatite. Consequently, the excess carboxyl groups in the Fe_3O_4-rGO nanocomposites likely suppress the apatite formation.

3.2 *In vitro* heat generation

Figure 3 shows the temperature change of the agar phantom under an alternating magnetic field. The phantom with a high Fe_3O_4 content was rapidly heated. In particular, the temperature of GF15 and F samples approached 100°C within approximately 2 min and melting of the phantom was also observed. The temperature of GF4 approached 60°C after 10 min. Table 1 shows the SAR values of the samples calculated from the

results of the heat generation measurements in Fig. 3. The SAR tended to increase as the Fe_3O_4 content increased.

As the Fe_3O_4 content increased, the nanocomposite not only rapidly generated heat under an alternating magnetic field, but also increased its SAR value. This indicates that the heat generation performance of Fe_3O_4 nanoparticles enhances with increase in Fe_3O_4 content in the nanocomposite. It has been previously shown that all the samples prepared in this study are superparamagnetic by a vibrating sample magnetometer [14]. Heat generation in superparamagnetic materials is known to occur mainly by Né el relaxation and Brown relaxation [1]. For the latter mechanism, the magnetic moment is relaxed by rotation of the particles themselves, such that the relaxation time becomes longer in environments where rotation is suppressed. For the case of samples with a high rGO content, the ion-ion interactions or ion-dipole interactions between Fe ions of Fe_3O_4 and carboxyl or hydroxyl group of rGO are increased, which suppresses vibrations of the nanoparticles and the contribution of Brown relaxation. This assumption is schematically illustrated in Fig. 4. Furthermore, the particle size of the

Fe_3O_4 became smaller as the content of rGO was increased [14]. This change increases the specific surface area and likely also promoted the interaction described above.

The saturation magnetization per unit mass values of the nanocomposites of GF2 (Fe_3O_4 content : 50.5%) and F have been reported to be 1.63 and 58.7 emu / g, respectively [14]. Therefore, the saturation magnetization per unit mass values of Fe_3O_4 of GF2 was calculated to be 3.23 emu / g (Fe_3O_4). This value is much smaller than that of pure Fe_3O_4, indicating that the presence of non-magnetic rGO reduces the magnetization of Fe_3O_4 itself. It has been suggested that the coating layer on the magnetic nanoparticles might reduce the saturation magnetization by a shielding effect [25]. These factors also adversely affect SAR and the heat generation properties of the present nanocomposites with high rGO content.

Magnetic nanocomposites with sufficient heat generation for hyperthermia treatment were obtained in the present study. However, increase in temperature up to 100°C has a risk of damage to surrounding healthy tissues. Appropriate control in frequency and strength of alternating magnetic field is needed for medical applications because Fe_3O_4 has high Curie temperature (580°C).

It is reported that not only rGO [7] but also Fe_3O_4 [26] has good cytocompatibility when its concentration was around 0.1 mg/mL. It is therefore expected that the Fe_3O_4-rGO may also have it. On the other hand, *in vitro* cytotoxicity of the nanoparticles is governed by its particle size and state of aggregation [27,28]. Further studies on biological properties of the present nanoparticles are needed in future.

4. Conclusion

We found that the apatite-forming ability in SBF and heat generation characteristics of Fe_3O_4-rGO nanocomposites were highly dependent on their composition. Namely, both the amount of apatite formed and the heat generation ability of the Fe_3O_4 nanoparticles per unit mass increased as their Fe_3O_4 content was increased. Therefore, we clarified that a high Fe_3O_4 content is effective for optimizing both osteoconductivity and heat generation characteristics under an alternating magnetic field.

References

1. B. Jeyadevan, Present Status and Prospects of Magnetite Nanoparticles-based

Hyperthermia, J. Ceram. Soc. Japan, 118 (2010) 391–401.

2. M. Kawashita, K. Sadaoka, T. Kokubo, T. Saito, M. Takano, N. Araki, M. Hiraoka, Enzymatic Preparation of Hollow Magnetite Microspheres for Hyperthermic Treatment of Cancer, J. Mater. Sci.: Mater. Med., 17 (2006) 605–610.

3. T. Miyazaki, A. Miyaoka, E. Ishida, Z. Li, M. Kawashita, M. Hiraoka, Preparation of Ferromagnetic Microcapsules for Hyperthermia Using Water/oil Emulsion as a Reaction Field, Mater. Sci. Eng. C 32 (2012) 692–696.

4. Y. Ebisawa, F. Miyaji, T. Kokubo, K. Ohura, T. Nakamura, Bioactivity of Ferromagnetic Glass-ceramics in the System FeO-Fe_2O_3-CaO-SiO_2, Biomaterials 18 (1997) 1277–1284.

5. S. Murakami, T. Hosono, B. Jeyadevan, M. Kamitakahara, K. Ioku, Hydrothermal Synthesis of Magnetite/hydroxyapatite Composite Material for Hyperthermia Therapy for Bone Cancer, J. Ceram. Soc. Japan 116 (2008) 950–954.

6. A. Matsumine, K. Kusuzaki, T. Matsubara, K. Shintani, H. Satonaka, T. Wakabayashi, S. Miyazaki, K. Morita, K. Takegami, A. Uchida, Novel

Hyperthermia for Metastatic Bone Tumors with Magnetic Materials by Generating an Alternating Electromagnetic Field, Clin. Exp. Metastasis 24 (2007) 191–200.

7. M. Kalbacova, A. Broz, J. Kong, M. Kalbac, Graphene Substrates Promote Adherence of Human Osteoblasts and Mesenchymal Stromal Cells, Carbon 48 (2010) 4323–4329.

8. Y. Yang, A.M. Asiri, Z. Tang, D. Du, Y. Lin, Graphene Based Materials for Biomedical Applications, Mater. Today 16 (2013) 365–373.

9. M. Mehrali, E. Sadeghinezhad, A.R. Akhiani, S.T. Latibari, H.S.C. Metselaar, A.S. Kherbeet, M. Mehrali, Heat Transfer and Entropy Generation Analysis of Hybrid Graphene/Fe_3O_4 Ferro-nanofluid Flow Under the Influence of a Magnetic Field, Powder Tech. 308 (2017) 149–157.

10. M. Tanahashi, T. Matsuda, Surface Functional Group Dependence on Apatite Formation on Self-assembled Monolayers in a Simulated Body Fluid, J. Biomed. Mater. Res. 34 (1997) 305–315.

11. M. Kawashita, M. Nakao, M. Minoda, H.M. Kim, T. Beppu, T. Miyamoto, T. Kokubo, T. Nakamura, Apatite-forming Ability of Carboxyl Group-containing

Polymer Gels in a Simulated Body Fluid, Biomaterials 24 (2003) 2477–2484.

12. A. Sugino, T. Miyazaki, C. Ohtsuki, Apatite-forming Ability of Polyglutamic Acid Hydrogels in Body Environment, J. Mater. Sci.: Mater. Med. 19 (2008) 2269–2274.

13. P.S. Teo, H.N. Lim, N.M. Huang, C.H. Chia, I. Harrison, Room Temperature in situ Chemical Synthesis of Fe_3O_4/graphene, Ceram. Int. 38 (2012) 6411–6416.

14. P.S. Teo, A. Pandikumar, H.N. Lim, N.M. Huang, C.H. Chia, Magnetically Separable Reduced Graphene Oxide/iron Oxide Nanocomposite Materials for Environmental Remediation, Catal. Sci Tech. 4 (2014) 4396–4405.

15. N. Ye, Y. Xie, P. Shi, T. Gao, J. M, Synthesis of Magnetite/graphene oxide/chitosan Composite and Its Application for Protein Adsorption Mater. Sci. Eng. C, 45 (2014) 8–14.

16. Y. Xue, H. Chen, D. Yu, S. Wang, M. Yardeni, Q. Dai, M. Guo, Y. Liu, F. Lu, J. Qu and L. Dai, Oxidizing metal ions with graphene oxide: the in situ formation of magnetic nanoparticles on self-reduced graphene sheets for multifunctional applications, Chem. Commun. 47 (2011) 11689–11691.

17. S.B. Cho, K. Nakanishi, T. Kokubo, N. Soga, C. Ohtsuki, T. Nakamura, T. Kitsugi, T. Yamamuro, Dependence of Apatite Formation on Silica Gel on Its Structure: Effect of Heat Treatment, J. Am. Ceram. Soc. 78 (1995) 1769–1774.

18. M. Kawashita, S. Domi, Y. Saito, M. Aoki, Y. Ebisawa, T. Kokubo, T. Saito, M. Takano, N. Araki, M. Hiraoka, In vitro Heat Generation by Ferrimagnetic Maghemite Microsheres for Hyperthermic Treatment of Cancer under an Alternating Magnetic Field, J. Mater. Sci.: Mater. Med. 19 (2008) 1897–1903.

19. Z. Li, M. Kawashita, N. Araki, M. Mitsumori, M. Hiraoka, M. Doi, Magnetite Nanoparticles with High Heating Efficiency for Application in Hyperthermia of Cancer, Mater. Sci. Eng. C 30 (2010) 990–996.

20. G. Naik, S. Krishnaswamy, Photoreduction and Thermal Properties of Graphene-Based Flexible Films, Graphene 6 (2017) 27–40.

21. Y. Kato, T. Yokoi, E. Shin, I.Y. Kim, M. Kawashita, K. Kikuta, C. Ohtsuki, Calcium Phosphate-forming Ability of Magnetite and Related Materials in a Solution Mimicking in vivo Conditions, J. Asian Ceram. Soc. 3 (2015) 44–49.

22. M. Tavafoghi, N. Brodusch, R. Gauvin, M. Cerruti, Hydroxyapatite Formation on

Graphene Oxide Modified with Amino Acids: Arginine Versus Glutamic Acid, J. R. Soc. Interface 13 (2016) 20150986.

23. S.H. Rhee and J. Tanaka, Effect of citric acid on the nucleation of hydroxyapatite in a simulated body fluid, Biomaterials 20 (1999) 2155-2160.

24. T. Ichibouji, T. Miyazaki, E. Ishida, A. Sugino, C. Ohtsuki, Apatite Mineralization Abilities and Mechanical Properties of Covalently Cross-linked Pectin Hydrogels, Mater. Sci. Eng. C 29 (2009) 1765–1769.

25. M. Mikhaylova, D.K. Kim, C.C. Berry, A. Zagorodni, M. Toprak, A.S.G. Curtis, M. Muhammed, BSA Immobilization on Amine-Functionalized Superparamagnetic Iron Oxide Nanoparticles, Chem. Mater. 16 (2004) 2344-2354.

26. A.K. Gupta, S. Wells, Surface-modified Superparamagnetic Nanoparticles for Drug Delivery: Preparation, Characterization, and Cytotoxicity Studies, IEEE Trans. Nanobioscience. 3 (2004) 66-73.

27. F. Watari, S. Abe, C. Koyama, A. Yokoyama, T. Akasaka, M. Uo, M. Matsuoka, Y. Totsuka, M. Esaki, M. Morita, T. Yonezawa, Behavior of in vitro, in vivo and Internal Motion of Micro/nano Particles of Titanium, Titanium Oxides and Others,

J. Ceram. Soc. Japan 116 (2008) 1-5.

28. A. Albanese, W.C.W. Chan, Effect of Gold Nanoparticle Aggregation on Cell Uptake and Toxicity, ACS Nano 5 (2011) 5478–5489.

Table 1 Zeta potentials (n=3), Ca/P molar ratio (n=3) on the surfaces after 2-h immersion in SBF and calculated SAR values (n=1) of the samples. The data was expressed as (mean)±(standard deviation)

Sample	Zeta potential (mV)	Ca/P	SAR (W/[g of Fe])
GF4	−21.6±0.746	25.0±5.16	0.141
GF10	−8.42±0.085	8.80±2.45*	0.618
GF15	−1.94±0.395	8.95±4.77*#	1.65
F	8.38±1.17	8.37±3.70*#†	1.60

*p<0.05 vs GF4, #p>0.5 vs GF10, †p>0.5 vs GF15

Figure captions

Figure 1 SEM images of the sample surfaces immersed in SBF for 7 days.

Figure 2 TF-XRD patterns of the sample surfaces immersed in SBF for 7 days.

Figure 3 Temperature change of agar phantoms under an alternating magnetic field.

Figure 4 Schematic illustration of the interaction between Fe_3O_4 and rGO.

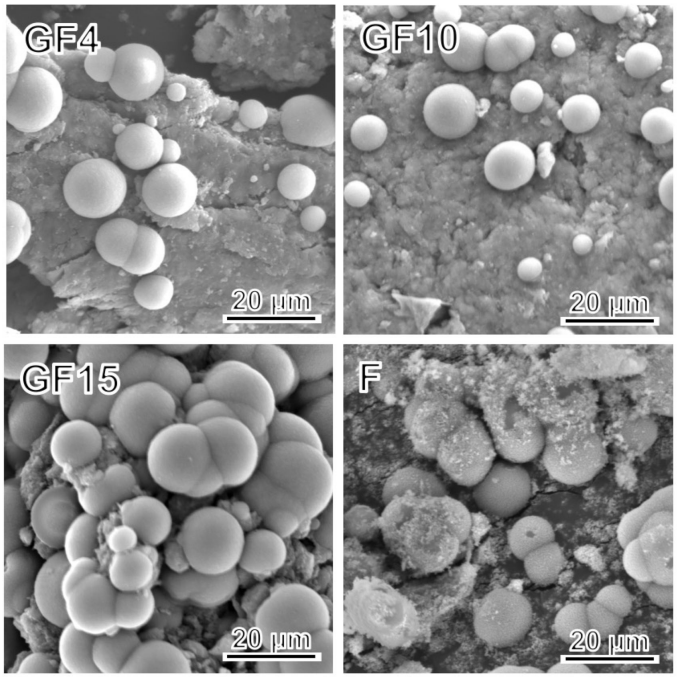

Fig. 1

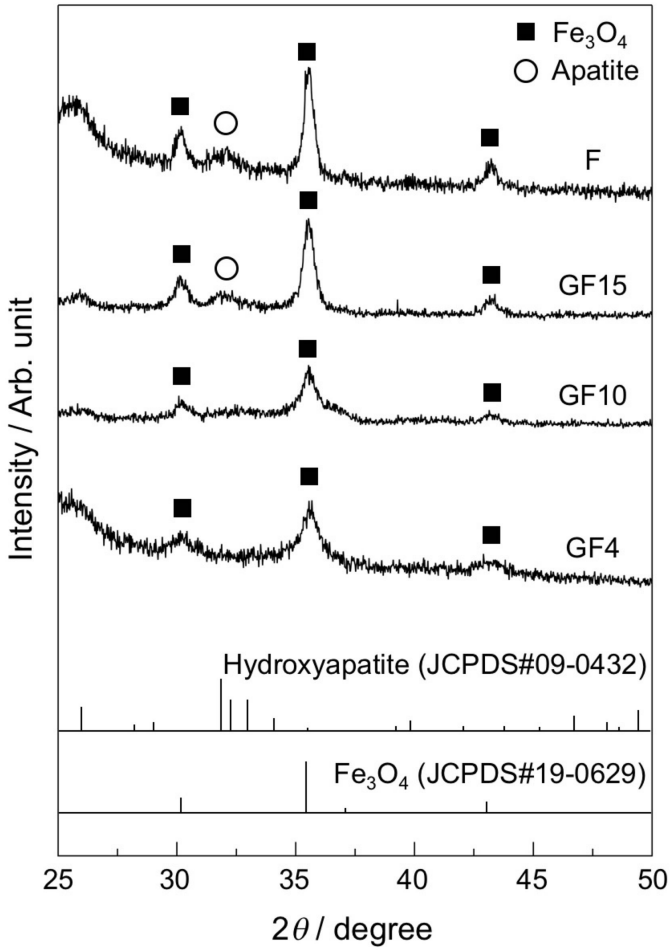
■ Fe_3O_4
○ Apatite
F
GF15
GF10
GF4
Intensity / Arb. unit
Hydroxyapatite (JCPDS#09-0432)
Fe_3O_4 (JCPDS#19-0629)
25
30
35
40
45
50
2θ / degree

Fig. 2

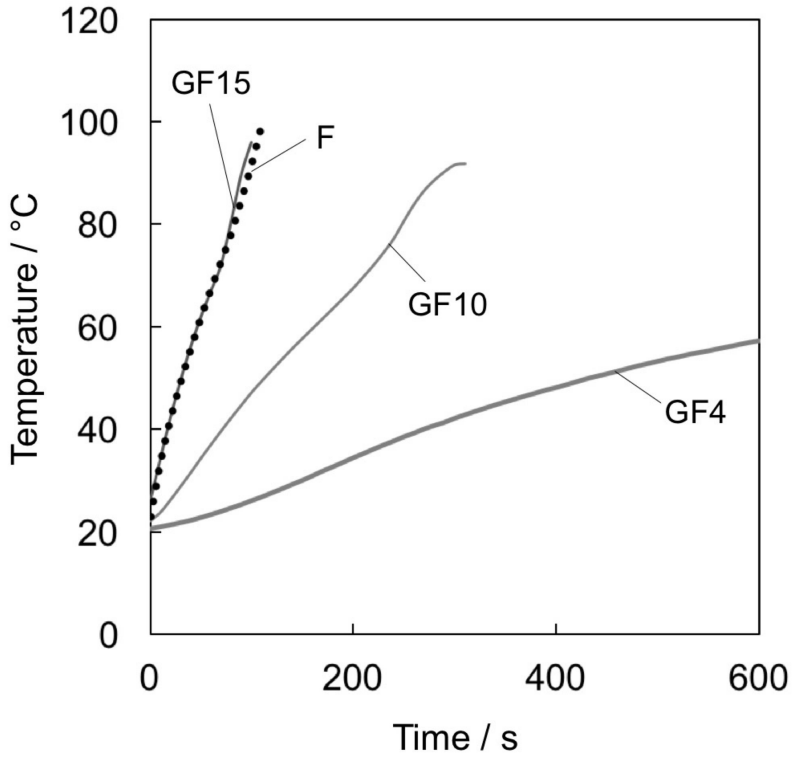
120
100
80
60
40
20
0
Temperature / °C
GF15
F
GF10
GF4
0
200
400
600
Time / s

Fig. 3

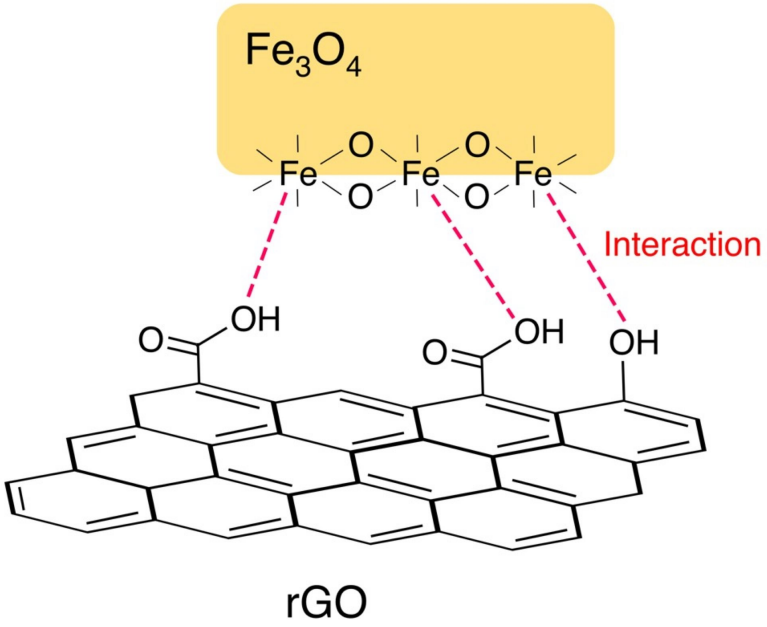

Fig. 4

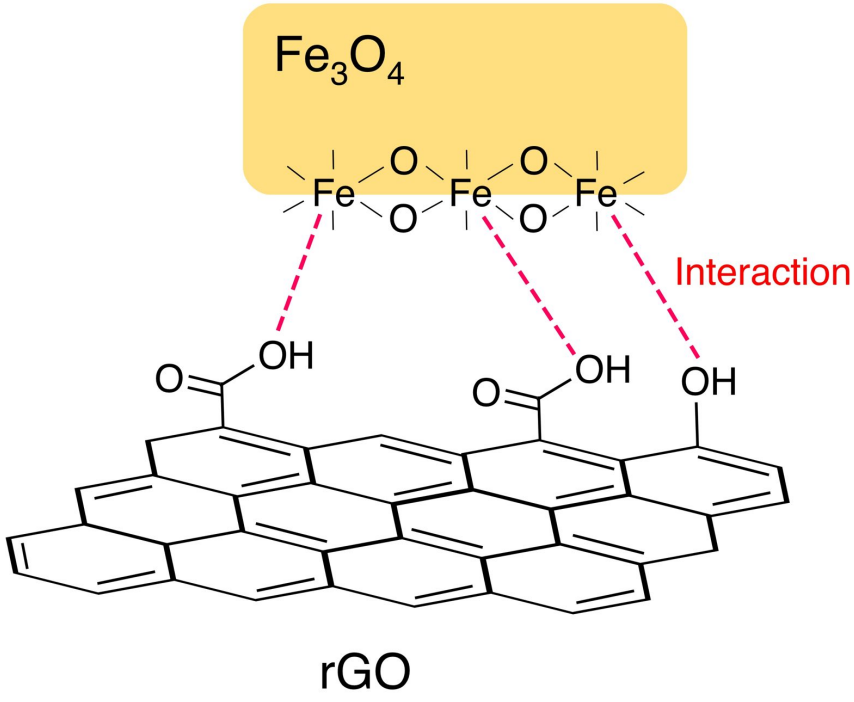
Fe3O4
Fe
O
Fe
O
Fe
O
O
O
Interaction
OH
O
OH
O
OH
rGO

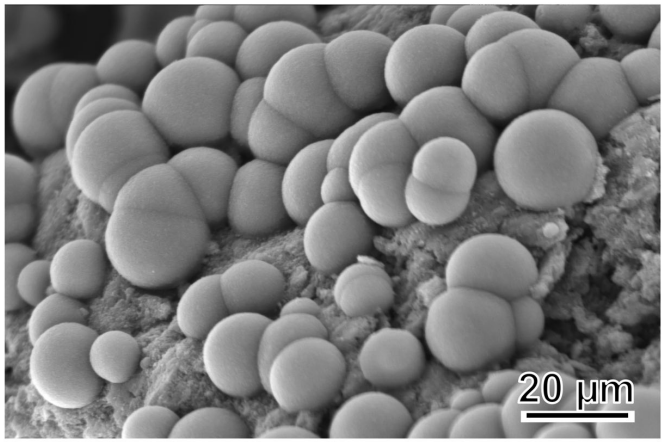
20 μm

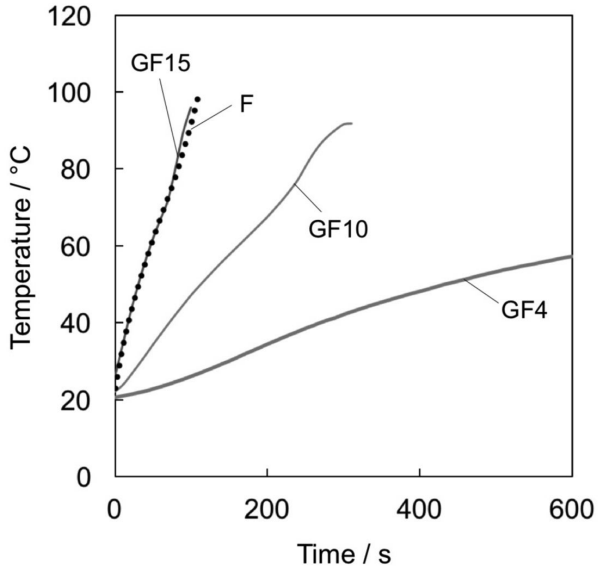
120
100
80
60
40
20
0
Temperature / °C
GF15
F
GF10
GF4
0
200
400
600
Time / s